

Hybrid Sensor in the Loop Approach for Generating Synthetic Event Imager Data of Melt Pool Dynamics

Anthony Starleaf*, Aidan Gribble*, Nicholas Bruns*, David Mascareñas*, Mahtab Heydari†, Bruce Tai†

*Los Alamos National Laboratory, Los Alamos, NM 87545

†Texas A&M University, College Station, TX 77840

Abstract

High dynamic range neuromorphic event based imagers show promise for high-speed, memory-efficient, in process monitoring of additive manufacturing. These imagers can observe the high light intensity environment of the melt pools while reducing memory requirements by only detecting change in log light intensity of each pixel. Advances in machine learning suggest that data augmentation with synthetic data is often desirable when considering complex dynamic systems where data collection can be expensive and there is potential for high consequence longtail events (e.g., driverless vehicles). However, generating synthetic event data presents challenges in accurately modeling phenomena such as event imager noise, high dynamic range/Fourier optics effects, and multi-time scale dynamics. To make progress on simulating high-fidelity event data for in-process monitoring and control of melt pools, we propose a hybrid sensor in the loop approach that leverages emerging commercially available high speed monitoring technology. Literature suggests that melt pool depth can be inferred from surface oscillations. In this study, we examine the suitability of using a hybrid sensor in the loop approaches to generate synthetic event data, representative of multi-time scale dynamics of melt pools in order to infer 3D melt pool geometry.

Introduction

There is currently great interest in enabling in-process monitoring and control for metal additive manufacturing in order to control melt pool size, and detect anomalies such as wire feed errors as well as lack of fusion defects. The hope is that by enabling in-process monitoring and control, the need for expensive post-fabrication non-destructive evaluation (NDE) for verifying part quality can be mitigated. Post-fabrication NDE can be particularly challenging for additive manufacturing on account of the complicated geometries that additive manufacturing can generate. One of the largest challenges with enabling in-process monitoring has been addressing the generation of large amounts of data during the course of the build. Large amounts of data come from having multiple sensor modalities observing a melt pool over long periods of time (hours to days). Furthermore, melt pools are known to feature sub-millisecond dynamics [1], requiring high framerates to observe, which further increases data storage requirements and results in the need for additional computing resources. Benjamin Brown led efforts to try to mitigate the need for large amounts of sensor data by specifying a “lightweight approach to on-machine monitoring. [2]” This work identified in-line photodiode detection, visible wavelength imaging, machine data monitoring, and acoustic sensing as a memory-efficient suite of measurements to enable in-process monitoring. Of these, visible wavelength imaging often introduces the highest demands on computational resources. Researchers often use high-speed video cameras for scientific work, but

current use of high-speed cameras for in-process monitoring and control is impractical for routine operations on account of computational and memory requirements [1]. Another notable problem for conventional imagers is the need to operate in high dynamic ranges of light intensity. Conventional 8-bit imagers often suffer from oversaturation of pixels when observing melt pools. A good example of the oversaturation problem can be found in the work by Myers which tried to use conventional imagers to build a two-color pyrometer for melt pool temperature measurements [3]. This work demonstrates multiple examples where pixel oversaturation makes temperature measurement impractical. Meyers attempts to mitigate the pixel saturation challenge by using different exposure times over multiple runs. However, this approach is of questionable practicality for operational in-process monitoring. An illustration of the dynamic range issue associated with melt pool monitoring is shown in Figure 1. Here we see two frames captured during the electron beam additive manufacturing process during the same build, but with different levels of light illuminating the imager sensor. In Figure 1a., the level of light reaching the sensor is higher allowing the trailing edge of the melt pool to be seen. However, the number of pixels experiencing saturation is very large and a large part of the melt pool is not observable at all. In contrast, Figure 1b. has a lower level of light reaching the imager sensor. In this case, fewer pixels experience saturation, however the trailing edge of the melt pool cannot be observed. In this way the dynamic range of the imager inherently introduces tradeoffs associated with how much of the melt pool can be observed and under what conditions.

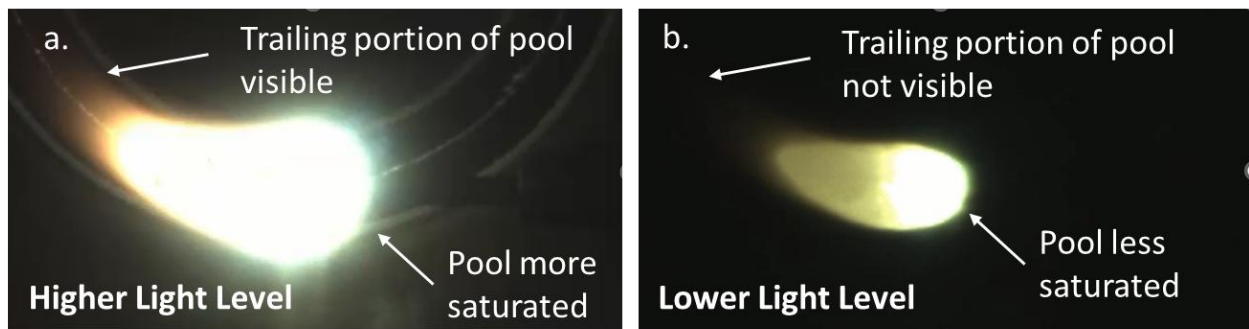


Figure 1 Illustration of the high dynamic range light intensity environment observed during electron beam additive manufacturing.

In 2022, Gothard Et al. [4] introduced the use of high-dynamic range neuromorphic event imagers for observing melt pools. Neuromorphic event imagers, [5], [6], [7], [8], [9], are fundamentally different from conventional imagers in that they only report data when the change in level of log light intensity at a pixel exceeds a pre-defined value. This detection occurs at the pixel hardware level. Fundamentally different architectures are used by these imagers to report these event changes at each pixel. As a result, these imagers are often able to observe fast phenomena with timescales on the millisecond to even sub-millisecond at interactive speeds. There is no waiting for data to download as would be the case with conventional high speed imagers. Each event consists of information on the pixel x-y location, the polarity of the change (increasing/decreasing) and a timestamp that has sub-millisecond resolution [10]. Because these imagers detect changes in log light intensity, they are reported to have dynamic ranges on the order of 120 dB. This makes them very attractive for monitoring melt pools. Particularly because they only detect changes and offer an opportunity to reduce data rates while still observing fast

phenomena. Additional work on observing melt pools with neuromorphic imagers can be found in [11], [12], [13]. Results to date suggest that neuromorphic event-based imagers offer a promising path forward for making in-process monitoring of melt-pools a reality.

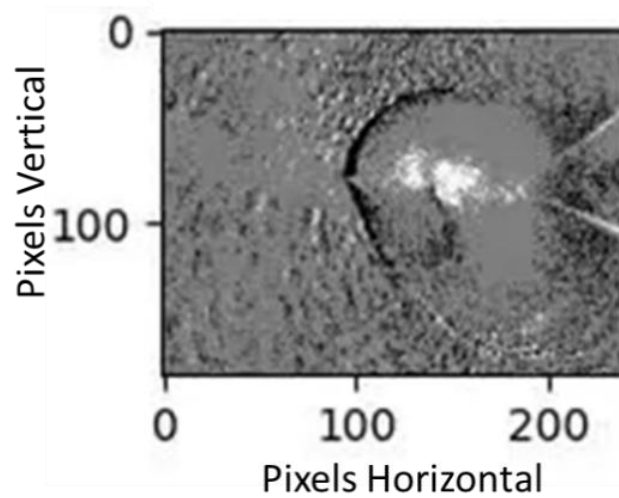


Figure 2 Example of a gas tungsten arc welder (GTAW) melt pool observed using a Davis240 neuromorphic imager with welding shade.

Melt Pool Dynamics from the Perspective of Neuromorphic Imagers

In prior work it has been reported that depth of melt pools can be estimated from vibrational behavior measured with a laser doppler vibrometer into the hundreds of Hertz [14]. More recently Jeon made use of a variety of optical measurements combined with artificial neural networks to estimate melt pool depth [15]. Dorn Et al. demonstrated that vibration mode shapes of a cantilever beam can be estimated from neuromorphic imager data. [16]. Taken together, these results suggest that it may be possible to estimate melt pool depth and other melt pool quantities relying primarily on efficient neuromorphic imager data. Currently we are in the process of exploring this possibility. A gas tungsten arc welder (GTAW)-based testbed has been assembled as shown in Figure 3. An example frame [4] formed from event data captured using a neuromorphic imager in this testbed is shown in Figure 4.

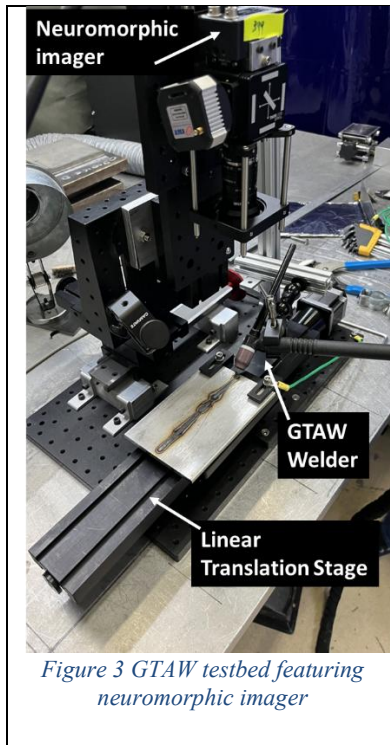


Figure 3 GTAW testbed featuring neuromorphic imager

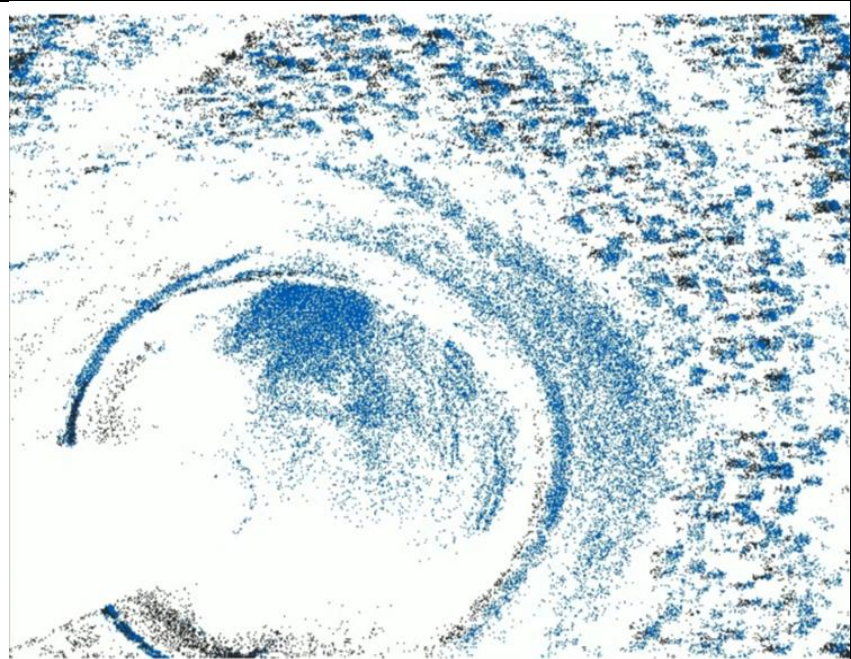


Figure 4 Example of a melt pool frame (640x480) that can be generated from neuromorphic imager data.

Testbeds can potentially speed up development cycles by facilitating data collection, particularly in cases where commercial equipment is expensive and difficult to access due to operational needs. Another significant issue with commercial platforms is that they are often closed-source, preventing ideal data capture. Testbeds can avoid these issues, but they still often lack a rate of data generation that is desirable for machine learning and reinforcement learning algorithms. In addition, capturing data for verification and validation from the testbeds can require expensive sensors, and there is still some uncertainty about the quality of the verification and validation data. Furthermore, for machine learning and reinforcement learning algorithms, there can be a large variety of different cases that must be observed to capture a sufficiently sophisticated model. Costs for labeling datasets can be quite high. Capturing different data for the combinatorial explosion of different cases can become very time consuming and expensive.

In the self-driving car and truck field it has become common to deal with the need for large training data sets by making use of synthetically generated data [17], [18], [19]. This data is well characterized, and the process of labeling training datasets is amenable to automation. A similar strategy would be desirable for in-process monitoring of additive manufacturing and welding applications. However, generating imager data for melt pools poses its own challenges. First is the high light intensity involved with melt pool formation. Second is the high solidification rates that would require rendering of frames at high FPS values. Third, melt pools are dynamic and so motion blur effects must be taken into account in a principled manner. Fourth, it is difficult to find literature on quantitatively characterizing the high dynamic range, high speed light environment. It is desirable to get more information on the high intensity light environment in order to ensure that modeling techniques associated with this environment have sufficient fidelity for algorithm development.

Challenges with Simulating Event Data

The features of event imagers that make them attractive for a variety of applications also make them challenging to simulate. Event imagers are able to simultaneously observe phenomena that is occurrent on the second time scale to the sub millisecond timescale. In contrast, current computer graphics techniques for photorealistic rendering have primarily focused on emulating human vision, and as a result most framerates are on the order to 30 to 60 frames per second. An event-imager on the other hand can observe phenomena over about 4 orders of timescales. If naively using conventional computer graphics techniques, a very large number of frames (10,000 frames per second at least) would need to be simulated in order to take advantage of the full temporal bandwidth of the event imager. This would be very computationally expensive. Furthermore, conventional ray trace-based rendering techniques do not capture motion blur. Event imagers do not really experience motion blur, but because event imagers inherently detect changes in log light intensity, there must be some consideration with respect to how motion manifests itself in the event detections.

Eclipse Data (10/14/23)

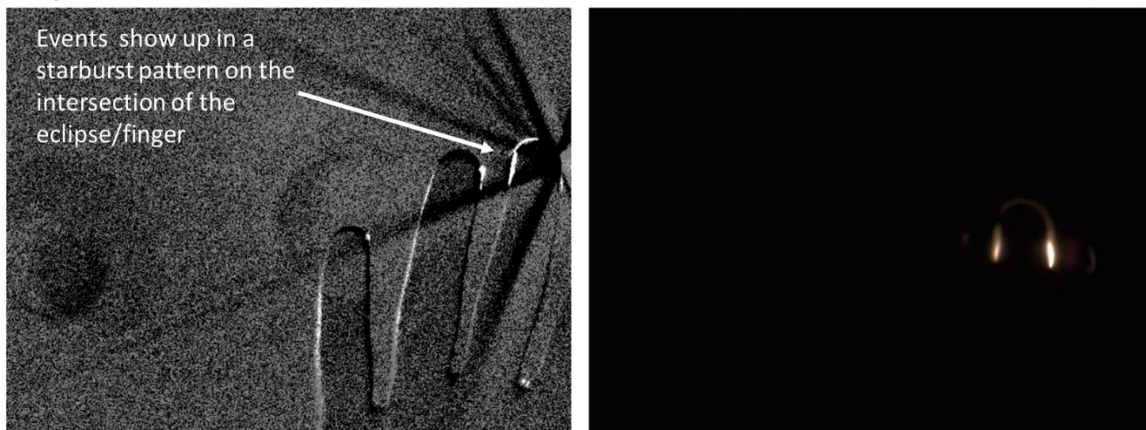


Figure 5 Event images have a high dynamic range (120 dB reported). They appear to observe Fourier optics effects that conventional imagers do not typically observe.

Another issue is addressing the noise characteristics of the event based imager. Prior work on the physical limits of event noise was done by Graca [20]. Graca found that the physical limit of a dynamic vision sensor event imager was limited to a theoretical minimum of 2X photon shot noise, and that biasing the imager with high photoreceptor bias and adequate source-follower bias approaches optical noise performance. In 2024 Arja Et al. cataloged a number of noise filtering benchmarks for event sensors, in particular in the context of satellite observations [21].

These prior works on noise focus on the scenario of low-light conditions. Observing melt pools is exactly the opposite because the light levels are very high. To the best knowledge of the authors, the noise behavior of current event imagers have not been characterized at the light intensity levels associated with melt pools. It is possible that unanticipated behaviors will manifest themselves at these high intensity levels. An example of this can be seen in Figure 5. Here an event imager and a conventional imager are being used to observe the sun during an eclipse. In this case, when the finger covers the eclipse it generates a “star burst” pattern of events. It is currently hypothesized that these events are a consequence of the point spread function of the

optics and the high dynamic range of the imager. The hypothesis is that these “star bust patterns” can be observed in this regime because the event imager has such a high dynamic range, and sufficient light is basically making it into the lower sidelobes of the point spread function of the optics to trigger an event. It is currently believed that the high dynamic range of the optics allows this phenomenon to be observed when it could not be observed for a conventional 8 bit imager. This is an example of an optical phenomenon that is not observed in conventional computer vision. It is possible that this and other noise/noise-like phenomena will present themselves in the extreme environment introduced by the melt pools.

Hybrid Neuromorphic Imager Setup

In order to address the issue of currently un-modeled and incompletely understood dynamics of the event imagers, we propose the use of emerging high framerate monitors ([22], [23], [24]) to display scenes that can be observed by the event based imagers. This approach enables a hybrid, sensor-in-the-loop architecture for capturing quasi-synthetically generated event data for algorithm development and capture of training data for artificial intelligence systems that leverage neuromorphic imaging.

The hybrid neuromorphic imager setup leverages the emergence of high framerate monitors typically used for video game applications. The monitor is a Dell Alienware AW2521h that runs at 240Hz via HDMI 2.1 or 360Hz via display port 2.1. For display port on high frequency monitors it is necessary to make sure to check that the specific version of display port being used for output from the graphics card is capable of the frame rate. Display port 2.1 is capable of 900Hz at 1080p, but 2.0 is only capable of 240Hz at 1080p. In this work we are using HDMI at 240 Hz.

An aluminum frame covered with a Musou Black felt fabric skin is used to enclose the monitor to reduce stray light being observed by the event imager. Opposite the monitor, imagers are set up to observe the test patterns displayed on the monitor. In this work we rely on a DVXplorer from IniVation. However, the current setup can facilitate having a conventional imager also view the screen through a beam splitter. Figure 6 shows the frame with the fabric removed in order to show how the experiments were set up. The design, bill-of-materials, and assembly of a similar experimental setup inspired by this design can be found in [25].

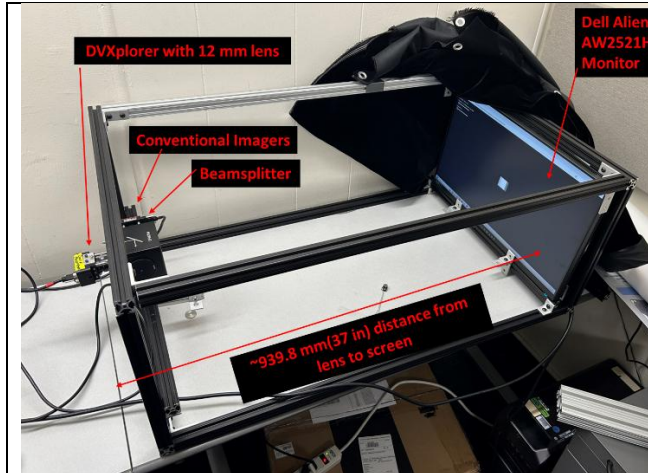


Figure 6 Hybrid neuromorphic imager-in-the-loop setup for generating simulated data for neuromorphic imagers. Outer Musou black felt covering removed to show internals.



Figure 7 Hybrid neuromorphic imager-in-the-loop setup for generating simulated data for neuromorphic imagers. Outer Musou black felt covering is used to reduce stray light entering the system.

Dynamic Systems Experiment

The current monitors are not able to emit sufficient light to exercise the high dynamic range characteristics of the event imagers. Instead, we start by focusing on the ability to characterize the temporal frequency measurement performance of the imagers in conjunction with the ability of the monitor to generate various temporal frequencies. This approach is motivated by prior work suggesting that melt pool dynamics can indicate information regarding melt pool depth [14].

Experiments

Several experiments were performed in order to validate the ability of the 240Hz monitor testbed to simulate oscillatory motion at different frequencies. To this end, three broad test cases were employed. The first such case was that of a circle dilating and contracting at a single frequency (Figure 8) according to Equation 1.

$$r = 200 \text{ px} + A \sin(2\pi ft) \quad (1)$$

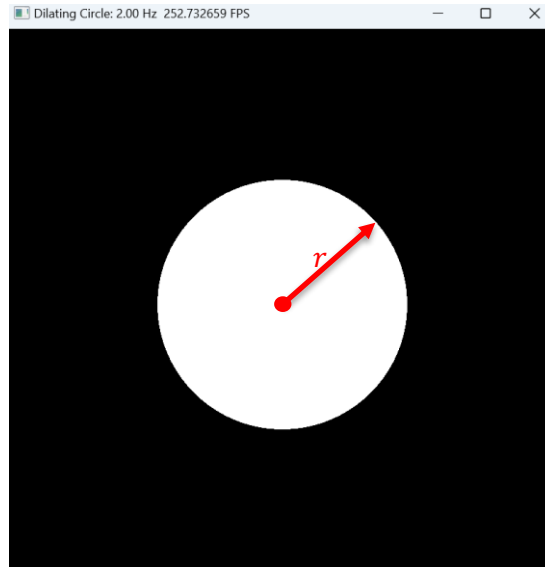


Figure 8 Example image of the dilating circle rendered on the 240Hz monitor.

The second test case was that of a square oscillating at a single frequency (Figure 9) according to Equation 2.

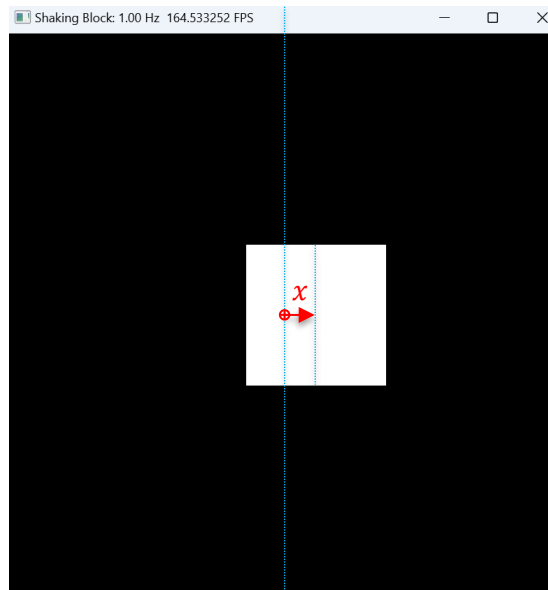


Figure 9 Example image of the oscillating square rendered on the 240Hz monitor.

$$x = A \sin(2\pi ft) \quad (2)$$

The third case was that of two rectangles overlaid in a “plus” shape (Figure 10), with the rectangles changing in size according to Equation 3.

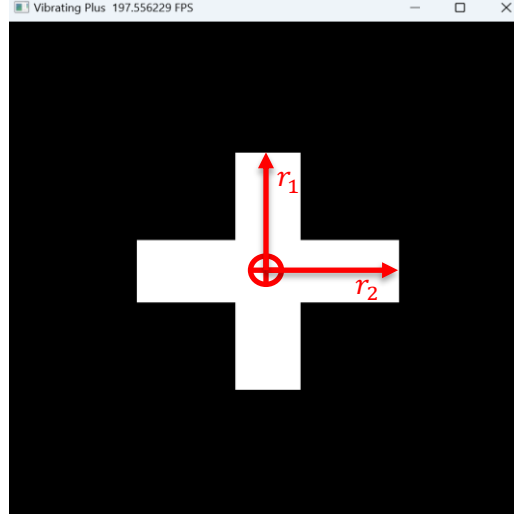


Figure 10 Example image of the dual-frequency “plus” rendered on the 240Hz monitor.

$$r_{1,2} = 200 \text{ px} + A \sin(2\pi f_{1,2} t) \quad (3)$$

In all three of the cases described above, animations were rendered for varying combinations of amplitudes A and frequencies f . For the “plus” case, f_1 was set to $0.5f_2$. For the remainder of the discussion, when discussing the frequency of the “plus” animation, we will be referring to the quantity f_2 (the frequency of the horizontal rectangle).

The frequencies used were as follows: $f \in F_0 = \{1, 2, 4, 8, 16, 32, 50, 55, 64, 128, 240\}$ Hz. The amplitudes tested were $A \in A_0 = \{5, 10, 20, 30\}$ px. Amplitudes are measured in monitor pixels. In the testbed’s current configuration, each camera pixel covers approximately 3 monitor pixels. Animations were created for all $(f, A) \in F_0 \otimes A_0$. These animations were run on the monitor and approximately 3 seconds of event data from each case was gathered.

This resulted in a total of 44 runs per case, for a total of 132 runs overall. It is worth noting that gathering this much data without the testbed (i.e. by manually exciting objects and recording them with the imager) would be difficult to repeat and prohibitively time-consuming. By using the testbed, it was possible to complete all 132 runs in approximately 30 minutes using a Python script to produce the animations and record the event data.

All tests were performed using a high-performance GPU-based renderer provided by the Taichi Python library and were recorded using a DVXplorer neuromorphic camera [10] with a 12 mm lens.

Analysis

In theory, the dominant frequency present in the event stream from each run should be equal to the frequency of excitation. To determine whether this was the case, a Fourier analysis was performed on the event streams. However, events imagers do not record a continuous range of intensity in the same way that conventional frame-based imagers do. They record the times at which intensity changes past a certain threshold, and the direction of that change. To that end, a suitable mathematical representation of an event stream must be developed before performing Fourier analysis. The equation below describes the representation that we selected.

$$p_{ij}(t) = \sum_k \delta(t - t_k) p_k \quad (4)$$

Here, $p_{ij}(t)$ represents the value of the event stream at time t and pixel (i, j) , $\delta(\cdot)$ is the Dirac delta function, k indexes all events recorded in the event stream, t_k is the time at which the event k occurred, and p_k is the polarity (+1 or -1) of event k . Taking the Fourier transform directly,

$$P_{ij}(\omega) = \int_{-\infty}^{\infty} \sum_k \delta(t - t_k) p_k e^{-j\omega t} dt \quad (5)$$

Note that the subscript j denotes an index, and the j in $e^{-j\omega t}$ denotes the imaginary number $j = \sqrt{-1}$. In this case, the sum and integral operators commute because their bounds are independent of one another, so

$$P_{ij}(\omega) = \sum_k \int_{-\infty}^{\infty} \delta(t - t_k) p_k e^{-j\omega t} dt \quad (6)$$

By the definition of the delta function, $\int_{-\infty}^{\infty} f(t) \delta(t - \tau) dt = f(\tau)$. Therefore,

$$P_{ij}(\omega) = \sum_k p_k e^{-j\omega t_k} \quad (7)$$

Equation 7 describes a pixel-wise Fourier transform of the event stream. This is useful when extracting mode shapes associated with various frequencies. However, we seek to identify a frequency which is dominant across all pixels of the resulting image. To this end, we use an average power spectral density function $\bar{P}(\omega)$, defined as follows.

$$\bar{P}(\omega) = \frac{1}{N_i N_j} \sum_{i=1}^{N_i} \sum_{j=1}^{N_j} P_{ij}(\omega) P_{ij}^*(\omega) \quad (8)$$

The dominant frequency in each event stream is found using the largest peak of $\bar{P}(\omega)$. For the “plus” case, the frequency associated with the second highest peak is also recorded, as this should correspond to the frequency of the vertical rectangle.

Results

The approach described above was applied to all 44 frequency-amplitude pairs for each of the three test cases. The predicted frequency was plotted against the true frequency of excitation for each case. These plots are given in Figure 11-Figure 13. In preliminary testing, it was determined that the maximum frequency which can be identified from an event-based recording of the monitor is approximately one-quarter of the monitor’s refresh rate. These experiments were carried out with the monitor’s refresh rate set to 240Hz, so a purple line is plotted at 60Hz to show the approximate location at which the dominant frequency present in the event stream no longer corresponds to the frequency of excitation. Note that this is likely due to properties of the monitor, rather than of the event imager.

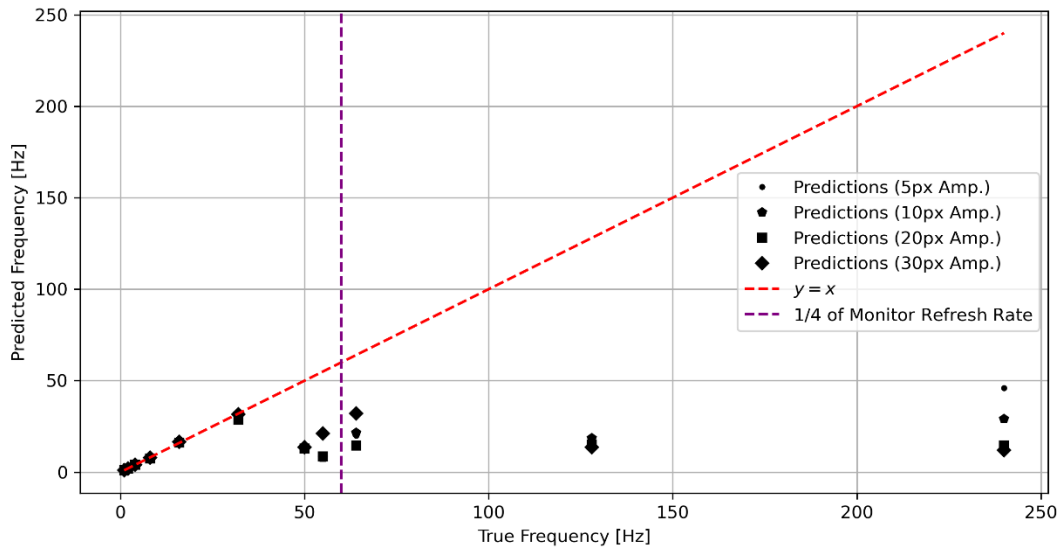


Figure 11 Performance plot for the dilating circle. The red line represents the theoretical behavior of a perfect predictor. Different shapes correspond to different amplitudes.

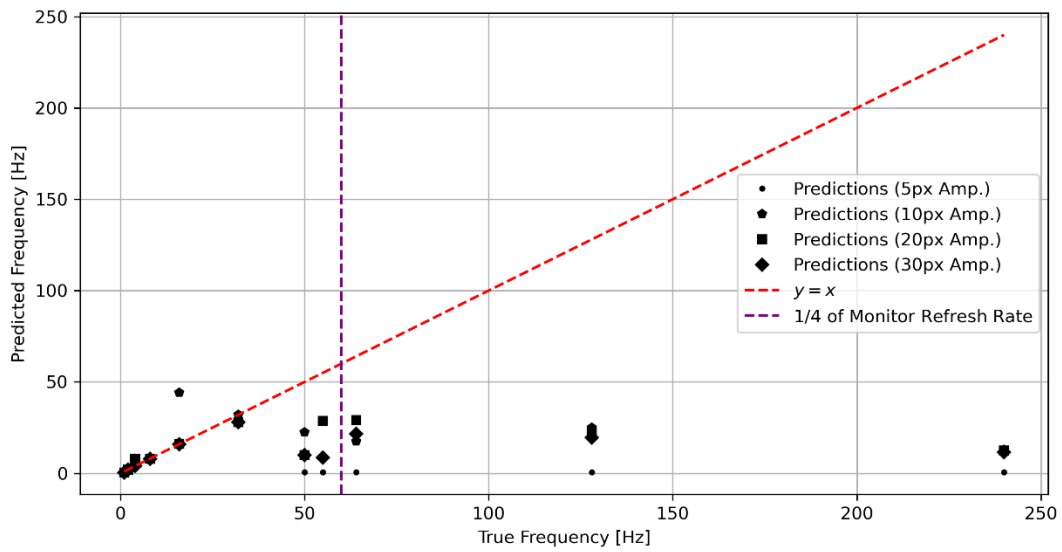


Figure 12 Performance plot for the oscillating square. Symbols retain the same meaning from Figure F4.

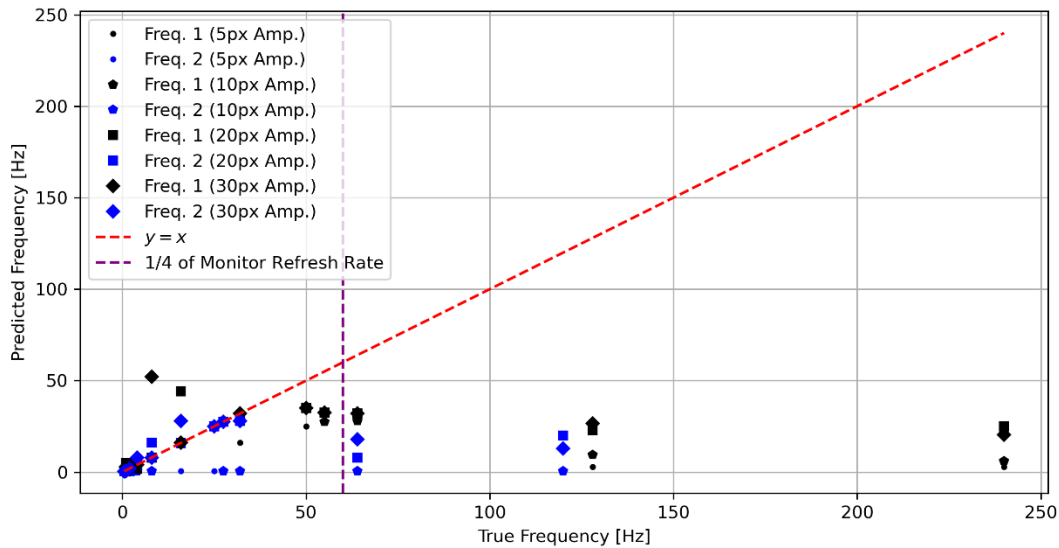


Figure 13 Performance plot for the two rectangles vibrating at different frequencies. Different shapes represent different amplitudes. Black markers represent the frequency of the horizontal rectangle. Blue markers represent the frequency of the vertical rectangle.

Discussion

Because of their asynchronous nature, event cameras are practically immune to aliasing. They sample the scene based on intensity changes, rather than at a fixed frequency and so are not affected by the Nyquist criterion. However, the monitor being used in the testbed displays the frames of each animation at a fixed frequency. As such, the *monitor* is subject to the Nyquist criterion, even though the imager is not. Therefore, the theoretical upper bound on the frequencies of physical phenomena which can be reliably simulated using this testbed is one-half of the monitor's refresh rate.

In practice, however, this upper bound is much lower. From Figure 11-Figure 13, it appears that the testbed in its current configuration is capable of simulating phenomena occurring below about 50Hz, which is nearly a quarter of the monitor's refresh rate. We hypothesize that this may be due to *ghosting (motion blur)* [23], or the fact that the pixels of the monitor may not fully dim back to zero by the next frame of the animation, producing artifacts that the event imager picks up on.

What follows is a very qualitative explanation of how ghosting may lower the effective upper bound on the frequencies that can be simulated by the monitor. If the pixels of the monitor take roughly as long to turn off as they do to turn on, then animated motion occurring at more than half of the monitor's refresh rate would be corrupted by ghosting. This reduces the monitor's effective refresh rate to approximately 120Hz. Applying the Nyquist criterion and treating 120Hz as the sample frequency, the highest frequency which can be represented by the monitor (without aliasing or ghosting) would be roughly 60Hz. This is what informed the location of the dashed purple line in Figures F4-F6, which roughly corresponds to the highest frequency at which the predicted frequencies match the true frequencies. It is worth noting that making use of the hybrid

approach has the potential collect data in a fast, low-cost, flexible manner that is repeatable, and allows us to be able to characterize differences between event imagers.

Future Work, Gallium Melt Pool Surrogates

In 2020 it was reported that preliminary results suggested that plausible mode shape information could be extracted from neuromorphic imager data of vibrating pools of molten gallium [26]. When pools of molten gallium are observed from overhead (Figure 14) one way the vibration signal associated with the melt pool manifests itself as a change in intensity at each pixel. Simulating event data from scenes such as this would also be of interest for advancing in-process monitoring for additive manufacturing. In future work we plan to evaluate the suitability of using high framerate monitors to simulate event data for overhead melt pool scenarios. We anticipate we will start this work by using Bessel functions (Figure 15) as a simplified model for melt pool dynamics.

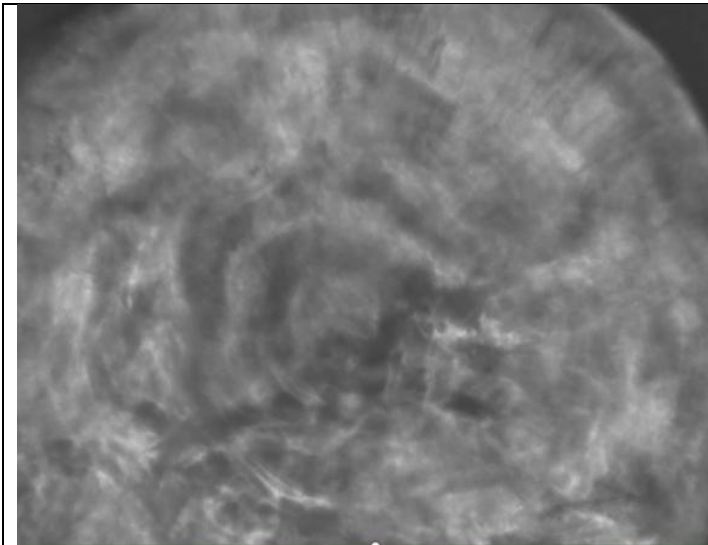


Figure 14 Image of a vibrating gallium melt pool observed with a conventional imager

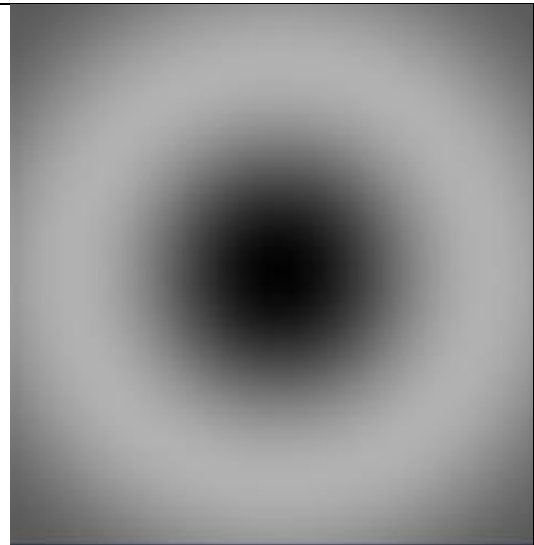


Figure 15 Simulated Bessel functions

Conclusions

It is anticipated that as the framerates of monitors continue to increase, high framerate monitors will become increasingly attractive for generating hybrid event data that leverages the flexibility of simulation while incorporating the true performance of the neuromorphic imagers into the test. Monitors with speeds of 1000 Hz have been reported [27]. It is perhaps worth noting that for hybrid neuromorphic imager-in-the-loop systems of this nature, it thus far seems desirable to have a monitor with a framerate on the order of 6X or more faster than the fastest dynamics in the scene. In future work it would also be advantageous if characterization for neuromorphic imagers could somehow incorporate high-dynamic range light sources in order to include high dynamic range phenomena occurring with sub-millisecond timescales into the testing. Ultimately it will be most practical if events can be simulated in a completely computational manner. However, to the best knowledge of the PI there is no event simulator that renders events across

disparate time scales and dynamic ranges. Furthermore, the noise behavior of these imagers is still not fully understood. Until these computational issues are addressed, a hybrid imager-in-the-loop approach is an attractive option for generating event data for algorithm development, obtaining training data for deep learning, and characterizing event imagers. In addition, it is anticipated that the hybrid approach will be a useful stepping stone that will yield insights to help enable fully computational modeling of event imagers observing high dynamic range, fast scenes. An additional advantage of the proposed approach is that it can greatly reduce the time for data collection as well as aid in characterizing variability between event imagers. In future work we plan to also look more rigorously at how events generated by the screen of a spatially oscillating block compare with event measurements captured from a physically oscillating Teflon cube.

Acknowledgements

This paper was supported by the Laboratory Directed Research and Development program of Los Alamos National Laboratory under project number 20250620MFR, 20220494MFR, 20220426ER, 20190547MFR as well as other funding sources internal to Los Alamos National Laboratory. Los Alamos National Laboratory is operated by Triad National Security, LLC, for the National Nuclear Security Administration of US Department of Energy (Contract No. 89233218CNA000001). The DVS/DAVIS technology was developed by the Sensors group of the Institute of Neuroinformatics (University of Zurich and ETH Zurich), which was funded by the EU FP7 SeeBetter project (grant 270324). We would like to acknowledge the help of Amber Black and Michael Torrez with the data collection for this project. Mahtab Heydari is supported by the LANL-TAMUS Graduate Fellowship Program, This work is partially supported by the NLO SEED grant program. We would like to acknowledge the help of Andre Green, with collecting some of the data and capturing some of the images.

References

- [1] P. A. Hooper, "Melt pool temperature and cooling rates in laser powder bed fusion," *Additive Manufacturing*, vol. 22, pp. 548-559, 2018.
- [2] C. Lough, J. Zettwoch, N. Welch and B. Brown, "Evaluation of Mechanical Performance as Indicated by Lightweight In-Situ Monitoring Sensor Modalities in LPBF," in *International Conference on Advanced Manufacturing*, Atlanta, GA, 2024.
- [3] A. J. Myers, G. Quirarte, F. Ogoke, B. M. Lane, S. Z. Uddin, A. B. Farimani, J. L. Beuth and Jonathan A. Malen, "High-resolution melt pool thermal imaging for metals additive manufacturing using the two-color method with a color camera," in *Additive Manufacturing*, Washington DC, 2023.
- [4] A. Gothard, D. Jones, A. Green, M. Torrez, A. Cattaneo and D. Mascareñas, "Digital coded exposure formation of frames from event-based imagery," *Digital coded exposure formation of frames from event-based imagery*, vol. 2, no. 014005, 2022.
- [5] M. Mahowald and C. Meade, "The Silicon Retina," *Scientific America*, vol. 264, no. 5, pp. 76-82, 1991.
- [6] P. Lichtsteiner, P. C. and D. T., "A 128 x 128 120 dB 15 μ s Latency Asynchronous Temporal Contrast Vision Sensor," *IEEE J. Solid-State Circuits*, vol. 43, no. doi: 10.1109/JSSC.2007.914337, pp. 566-576, 2008.

- [7] M. Mahowald and T. Delbruck, "Cooperative Stereo Matching Using Static and Dynamic Image Features," in *The Kluwer International Series in Engineering and Computer Science*, Springer, Boston, MA, 1989, pp. 213-238.
- [8] C. Mead, "Neuromorphic Electronic Systems," *Proceedings of the IEEE*, vol. 78, no. 10, pp. 1629 - 1636, 1990.
- [9] C. Mead and M. Ismail, *Analog VLSI and Neural Systems*, New York, NY: The Springer International Series in Engineering and Computer Science, 1989.
- [10] Inivation, "Specifications - Current Models," 2022. [Online]. Available: <https://inivation.com/wp-content/uploads/2023/02/2022-09-iniVation-devices-Specifications.pdf>. [Accessed 12 May 2023].
- [11] D. Mascareñas and A. Green, "On the use of event-based change detection neuromorphic imagers for in-process monitoring of additive manufacturing," in *Solid Freeform Fabrication 2024: Proceedings of the 35th Annual International Solid Freeform Fabrication Symposium*, Austin, Tx, 2024.
- [12] D. D. L. Mascareñas and A. W. Green, "Demonstration of Neuromorphic Event-Based Imagers for Optical Measurement of Melt Pools for Additive Manufacturing and Welding Diagnostics," in *Computer Vision & Laser Vibrometry, Vol. 6*, Orlando, FL, 2024.
- [13] D. Mascareñas, A. Green, A. Liao, M. Torrez, A. Cattaneo, A. Black, J. Bernardin and G. Kenyon, "Demonstrating the Suitability of Neuromorphic, Event-Based, Dynamic Vision Sensors for In Process Monitoring of Metallic Additive Manufacturing and Welding," <https://arxiv.org/abs/2411.13108>, 2024.
- [14] G. Arroud, J. Ertveldt and P. Guillaume, "A proof-of-concept analysis relating dimensions of a melt pool to its vibrational behavior to control a laser-based additive manufacturing process," in *Procedia CIRP*, 2020.
- [15] I. Jeon, P. Liu and H. Sohn, "Real-time melt pool depth estimation and control during metal-directed energy deposition for porosity reduction," in *The International Journal of Advanced Manufacturing Technology*, 2023.
- [16] C. Dorn, S. Dasari, Y. Yang, C. Farrar, G. Kenyon, P. Welch and D. Mascarenas, "Efficient Full-Field Vibration Measurements and Operational Modal Analysis Using Neuromorphic Event-Based Imaging," *Journal of Engineering Mechanics*, vol. 177, no. 7, pp. [https://doi.org/10.1061/\(ASCE\)EM.1943-7889.000144](https://doi.org/10.1061/(ASCE)EM.1943-7889.000144), 2018.
- [17] H. L. Lu, "Accelerating Autonomous Vehicle Development With OpenUSD Virtual Worlds," in *SIGGRAPH 2024*, 2024.
- [18] V. Serritella, V. Lundqvist, M. Webb, T. Shaw, R. Niu, Z. Repasky, R. Graf and M. Wrenninge, "A Procedural Production System for Autonomous Vehicle Simulation," in *SIGG, SIGGRAPH '24: ACM SIGGRAPH 2024 Talks*, 2024.
- [19] Z. Song, Z. He, X. Li, Q. Ma, R. Ming, Z. Mao, H. Pei, L. Peng, J. Hu, D. Yao and Y. Zhang, "Synthetic Datasets for Autonomous Driving: A," <https://arxiv.org/pdf/2304.12205v2>, 2024.
- [20] R. Graca, B. McReynolds and T. Delbruck, "Optimal biasing and physical limits of DVS event noise," in *IISS (Int. Image Sensors Society)*, Scotland, United Kingdom, 2023.

- [21] S. Arja, A. Marcireau, N. O. Ralph, S. Afshar and G. Cohen, "Noise Filtering Benchmark for Neuromorphic Satellites Observations," <https://arxiv.org/pdf/2411.11233v1>, Western Sydney University, 2024.
- [22] S. I. Lyapunov, I. I. Shoshina and I. S. Lyapunov, "Modeling the Critical Flicker Fusion Frequency in the Human Visual System," *Biophysics*, vol. 68, pp. 857-863, 2024.
- [23] K. Murakami, K. Miyashita and H. Miyachi, "A Study on the Relationship Between Refresh-Rate of Display and Reaction Time of eSports," in *Proceedings of the 15th International Conference on P2P, Parallel, Grid, Cloud and Internet Computing (3PGCIC-2020)*, 2021.
- [24] D. Klein, J. Spjut, B. Boudaoud and J. Kim, "The Influence of Variable Frame Timing on First-Person Gaming," <https://arxiv.org/pdf/2306.01691>, 2023.
- [25] D. Bluedorn, K. Brown, J. Johnson and D. Yazzie, "Optical Anechoic Chamber," <https://github.com/dhbluedorn/NeuromorphicPINN/blob/main/AssemblyInstructions/Assembly%20Instructions.pdf>, 2025.
- [26] C. Hayes, C. Schelle, G. Taylor, B. Martinez, G. Kenyon, T. Lienert, Y. Yang and D. Mascareñas, "Imager-Based Techniques for Analyzing Metallic Melt Pools for Additive Manufacturing," in *Special Topics in Structural Dynamics & Experimental Techniques, Volume 5, International Modal Analysis Conference*, 2020.
- [27] R. Larsen, "TCL unveils 1000Hz LCD, 14" QD-EL (NanoLED), 16" 8K LCD, and more," *flatpanelshd*, 17 May 2024.
- [28] K. Zheng, J. Sorenson, C. DeVilliers, A. Cattaneo, F. Moreu, G. Taylor and David Mascareñas, "Neuromorphic Data Processing for Event-Driven Imagery for Acoustic Measurements," in *International Modal Analysis Conference*, Orlando, FL, 2022.
- [29] K. Pearson, "On lines and planes of closest fit to systems of points in space," *Lond. Edinb. Dubl. Phil. Mag. J. Sci.*, vol. 2, no. 11, p. 559–572, 1901.